Cell Communication
and Signaling

RESEARCH

Alcohol and e-cigarette damage alveolar-epithelial barrier by activation of P2X7r and provoke brain endothelial injury via extracellular vesicles

Naveen Mekala[1], Jayshil Trivedi[1], Priyanka Bhoj[1], Namdev Togre[1], Slava Rom[1], Uma Sriram[1] and Yuri Persidsky[1*]

Abstract

Background Use of nicotine containing products like electronic cigarettes (e-Cig) and alcohol are associated with mitochondrial membrane depolarization, resulting in the extracellular release of ATP, and mitochondrial DNA (mtDNA), mediating inflammatory responses. While nicotine effects on lungs is well-known, chronic alcohol (ETH) exposure also weakens lung immune responses and cause inflammation. Extracellular ATP (eATP) released by inflammatory/stressed cells stimulate purinergic P2X7 receptors (P2X7r) activation in adjacent cells. We hypothesized that injury caused by alcohol and e-Cig to pulmonary alveolar epithelial cells (hPAEpiC) promote the release of eATP, mtDNA and P2X7r in circulation. This induces a paracrine signaling communication either directly or via EVs to affect brain cells (human brain endothelial cells - hBMVEC).

Methods We used a model of primary human pulmonary alveolar epithelial cells (hPAEpiC) and exposed the cells to 100 mM ethanol (ETH), 100 µM acetaldehyde (ALD), or e-Cig (1.75 µg/mL of 1.8% or 0% nicotine) conditioned media, and measured the mitochondrial efficiency using Agilent Seahorse machine. Gene expression was measured by Taqman RT-qPCR and digital PCR. hPAEpiC-EVs were extracted from culture supernatant and characterized by flow cytometric analysis. Calcium (Ca^{2+}) and eATP levels were quantified using commercial kits. To study intercellular communication via paracrine signaling or by EVs, we stimulated hBMVECs with hPAEpiC cell culture medium conditioned with ETH, ALD or e-cig or hPAEpiC-EVs and measured Ca^{2+} levels.

Results ETH, ALD, or e-Cig (1.8% nicotine) stimulation depleted the mitochondrial spare respiration capacity in hPAEpiC. We observed increased expression of P2X7r and TRPV1 genes (3-6-fold) and increased intracellular Ca^{2+} accumulation (20-30-fold increase) in hPAEpiC, resulting in greater expression of endoplasmic reticulum (ER) stress markers. hPAEpiC stimulated by ETH, ALD, and e-Cig conditioned media shed more EVs with larger particle sizes, carrying higher amounts of eATP and mtDNA. ETH, ALD and e-Cig (1.8% nicotine) exposure also increased the P2X7r shedding in media and via EVs. hPAEpiC-EVs carrying P2X7r and eATP cargo triggered paracrine signaling in human brain microvascular endothelial cells (BMVECs) and increased Ca^{2+} levels. P2X7r inhibition by A804598 compound normalized mitochondrial spare respiration, reduced ER stress and diminished EV release, thus protecting the BBB function.

*Correspondence:
Yuri Persidsky
yuri.persidsky@tuhs.temple.edu
Full list of author information is available at the end of the article

Conclusion Abusive drugs like ETH and e-Cig promote mitochondrial and endoplasmic reticulum stress in hPAEpiC and disrupts the cell functions via P2X7 receptor signaling. EVs released by lung epithelial cells against ETH/e-cig insults, carry a cargo of secondary messengers that stimulate brain cells via paracrine signals.

Keywords Ethanol, Electronic cigarette, Pulmonary alveolar epithelial cells, P2X7r, A804598, Extracellular vesicles, Paracrine signaling

Introduction

Electronic cigarettes (e-Cig) have gained popularity over combustible cigarettes, especially among young adults worldwide [1] and most of them are unaware that e-Cig vape contains higher nicotine concentration than combustible cigarettes does [2, 3]. Compared to combustible cigarette smokers and non-smokers, e-Cig smokers trigger early chronic inflammatory lung diseases [4]. Moreover, e-Cig vape induces the release of proinflammatory cytokines, including tumor necrosis factor alpha (TNF-α) and interleukin (IL)-1β, which promote chronic inflammation, pathologic changes in the lung parenchyma, and mitochondrial reactive oxygen species (ROS) buildup in lung epithelial cells [5, 6].

Although alcohol consumption is not directly linked to the onset of lung diseases, chronic alcohol exposure weakens lung responses to infections, particularly in the upper respiratory tract, resulting in poor immune response to pre-existing lung diseases or acquired infections [7–9]. Alcoholism is a major factor in the spread of community-acquired pneumonia and other acute respiratory complications, leading to thousands of deaths in the United States [10]. Excessive alcohol consumption alters mitochondrial structure [11] and reduces mitochondrial antioxidant glutathione levels, making mitochondria more susceptible to oxidative damage and ROS buildup, thus limiting ATP synthesis [12, 13]. Mitochondrial ROS accumulation instigates inflammation and DNA damage in lung epithelial cells [14]. Chronic alcohol exposure also stimulates purinergic P2X7 receptor (P2X7r), which activates NLRP3-mediated inflammasome in machrophages and releases extracellular ATP (eATP) as secondary messengers [15].

Lately, the association between inflammation and P2X7r has received much attention, with eATP release being a key source of inflammation [16, 17]. Furthermore, P2X7r activation promotes a sustained increase in intracellular calcium (Ca^{2+}) levels, which increases endoplasmic reticulum (ER) stress, eventually leading to inflammation [18, 19]. Our prior studies have demonstrated the influence of addictive drugs [ethanol (ETH) and e-Cig vape] on P2X7r activation, which facilitated intracellular Ca^{2+} accumulation and eATP release in brain microvascular endothelial cells (BMVECs). Pretreatment with the P2X7r antagonist A804598 (A80) restored homeostasis, prevented the blood-brain-barrier (BBB) compromise [20].

P2X7r activation by eATP also stimulates the generation of heterogeneous extracellular vesicles (EVs) that carry biomolecular cargoes that can mediate communication between similar (endocrine signaling) or different (paracrine signaling) cell types [21, 22]. EVs are bilayered membrane vesicles formed in an endosomal system and discharged into the extracellular space [23]. Although the cargo-carrying capacity of EVs is well established, the composition of the cargo does not always reflect the contents of the parental cells. Cells incorporate cargo into the EVs in a carefully controlled manner, reflecting the pathophysiological state of the cell [24]. During alcohol abuse, hepatocyte EVs transport broken mitochondrial DNA (mtDNA), which act as damage-associated molecular patterns (DAMPs), triggering inflammatory responses [25]. Similarly, EVs in patients with fatty liver conditions carry higher mtDNA and stimulate the innate immune response via the TLR-9 pathway [26]. In the past, the existence of diverse messengers, including proteins, lipids, nucleic acids, and cell organelles, has been well identified and characterized as EV cargo [27, 28], while data on eATP content as secondary messengers are sparse.

In our earlier study, we showed the effects of ETH and e-Cig on P2X7r regulation in BMVECs [20]. In this report, we assessed the neuroinflammatory effects of ETH and e-Cig vape on primary human pulmonary alveolar epithelial cells (hPAEpiC) via EVs. We specifically analyzed the effectiveness of P2X7r blockage by A80 on responses to e-Cig and ETH exposure, focusing on mito-stress regulation in hPAEpiC. We also examined its effect on intracellular Ca^{2+} accumulation, size and quantity of EVs released by the hPAEpiC. Finally, we examined the presence of P2X7r in the EVs, measured the eATP- and mtDNA-carrying capacity of hPAEpiC EVs, and tested their potential to mediate long-distance communication between hPAEpiC and BMVECs.

Materials and methods

Reagents/Kits

ETH 200 Proof, 99.5% pure aldehyde (ALD), and e-Cig (1.8% and 0% nicotine) were procured from Decon Laboratories Inc. (Cat. No. 2716, King of Prussia, PA, USA),

Mekala *et al. Cell Communication and Signaling*   (2024) 22:39

Page 3 of 16

ACROS Organics (Cat. No. 402788, Geel, Belgium), and Pure E-Liquids (Peterborough, PE11SB, UK), respectively. A80 was purchased from Tocris Bioscience (Cat. No. 4473, Bristol, UK) and dissolved in DMSO from Sigma-Aldrich (Cat. No. D5879, St. Louis, MI, USA). We purchased the luminescent ATP detection and colorimetric Ca^{2+} assay kits from Abcam (Cat. Nos. ab113849 and ab102505, respectively, Cambridge, UK). For EV isolation and capture, we used the ExoQuick-TC from SBI (Cat. No. EXOTC50A, Palo Alto, USA) and Tetraspanin Exo-Flow capture kit (Cat. No. EXOFLOW150A-1, Palo Alto, USA), respectively. anti-P2X7r antibodies (Alomone Labs, Jerusalem, Israel), were labelled using the Zip Alexa Fluor™ 647 rapid antibody labeling kit from Invitrogen (Cat. No. Z11235, Waltham, USA). The primary anti-rabbit antibodies for p-IRE1 (Cat. No. 3294T), p-ASK1 (Cat. No. 3765S), CD9 (Cat. No. 13174S), CD81 (Cat. No. 56039S), and beta-actin (Cat. No. 4967S) were procured from Cell Signaling (Danvers, MA, USA). Anti-rabbit Bax inhibitor-1 [BI-1] (Cat. No. ab18852) polyclonal antibodies were procured from Abcam (Cambridge, UK). Human purinergic receptor P2X, Ligand Gated Ion Channel 7 (P2RX7) ELISA Kit (Cat. No. RDR-P2RX7-Hu) obtained from Reddot Biotech (Houston, USA). Lyophilized recombinant human P2X7r protein (Cat. No. LS-G25681-10) procured from LS Bio (Lynnwood, USA). CellTiter 96® AQueous One Solution Cell Proliferation Assay kit (Cat.No. G3580) was procured from Promega (Madison, USA).

Cell cultures and treatments
hPAEpiC, acquired from Accegen (Cat. No. ABC-TC3770, Fairfield, USA), were cultured in hPAEpiC basal media (Cat. No. ABM-TM3770), supplemented with insulin-transferrin-selenium, epidermal growth factor, hydrocortisone, and 5% fetal bovine serum. hBM-VECs, provided by Dr. Pierre-Olivier Couraud, Institut Cochin, INSERM U1016, CNRS UMR 8104, Université Paris Descartes (Paris, France), [29] were cultured using EBM-2 basal medium (Cat. No. CC-3156), supplemented with EGM-2 SingleQuots (Cat. No. CC-4176) from Lonza Biosciences (St. Bend, USA). According to the experiment, both hPAEpiC and hBMVECs were cultured in 96-well plates, 6-well plates, 100-mm tissue culture plates, and T-75 and T-150 flasks, coated with bovine collagen from CELL applications. Inc (Cat. No. 123-100, San Diego, USA). Confluent hPAEpiC were pretreated with and without A80 (10 µM) for 1 h, followed by overnight stimulation with insults: ETH- (100 mM), ALD- (100 µM), or e-Cig (1.75 µg/mL of 1.8% and 0% nicotine)-conditioned media, with and without A80, respectively. A80 treated cells served as a P2X7r antagonist control. Unless mentioned, all experiments were carried out after overnight incubation. One hundred millimolar ETH concentration was selected based on the dose-dependent MTT assay (Supplementary Figure S1).

Mito-stress analysis
hPAEpiC (20,000 cells/well) were plated in a seahorse XF96 microplate from Agilent Technologies (Cat. No. 103794-100, Santa Clara, USA) and allowed to attach overnight. Four corner wells were left empty for background correction. The next day, the cells were treated with A80 (10 µM) for 1 h, followed by replacing old media with growth media conditioned with ETH, ALD, and e-Cig (1.8% or 0% nicotine) for overnight, with and without A80. The next morning, mitochondrial stress was measured using the Agilent Seahorse Cell Mito Stress Test Kit (Cat. No.103015-100, Santa Clara, USA). In brief, the growth media was carefully aspirated, and cells were washed twice in bicarbonate-free and phenol red-free DMEM, from Agilent (Cat. No. 103680-100, Santa Clara, USA), supplemented with 5.5 mM glucose, 1 mM pyruvate, and 2 mM glutamine. Lastly, 180 µL DMEM was added in all 96 wells including the four corner wells, and cells were kept in a non-CO_2 incubator at 37 ℃. After calibration of Seahorse cartridge, microplate was placed in the Seahorse analyzer, and basal oxygen consumption rates (OCR) were measured. Later, the cells were serially challenged with respiratory inhibitors- 2.5 µM oligomycin (ATP synthase inhibitor), 0.5 µM FCCP (mitochondrial uncoupler), and 0.5 µM rotenone/antimycin A (complex I/III inhibitor) and mitochondrial respiration levels were continuously recorded. After the assay, the spare respiratory capacity (SRC) was measured by subtracting the basal OCR from the maximal OCR.

Quantitative RT-PCR
Total RNA from hPAEpiC was isolated using the TRIzol™ reagent from Invitrogen (Cat. No. 15596026, Carlsbad, USA). Total RNA (400 ng) was converted into complementary DNA (cDNA) using the RT2 PreAMP cDNA Synthesis Kit (Cat. No. 330451, Qiagen, Germantown, MD, USA). TaqMan probes for human P2X7r (Cat. No. hs00175721), transient receptor potential vanilloid 1 (TRPV1; Cat. No. hs00218912), and GAPDH (Cat. No. hs02786624) were procured from Thermo Fisher (Waltham, USA). The cDNA was further probed for real-time qPCR using TaqMan Fast Advanced Master Mix (Cat. No. 4444557, Applied Biosystems, Waltham, USA). All reactions were performed in triplicate, and the relative fold-change of the P2X7r and TRPV1 gene expressions against the treatments were investigated using delta-delta-Ct (ddCt), and the values were normalized with ddCt values of GAPDH.

Mekala *et al. Cell Communication and Signaling*   (2024) 22:39

Page 4 of 16

Intracellular Ca²⁺ analysis

Confluent hPAEpiC, pre-treated with or without A80, were stimulated overnight with ETH, ALD, and e-Cig (1.8% or 0% nicotine) conditioned media, and intracellular Ca^{2+} levels were measured using Abcam Ca^{2+} assay kit (Cat. No. ab102505, Cambridge, UK) following the manufacturer's instructions.

Western blot analysis

Denatured proteins from hPAEpiC were separated using SDS-polyacrylamide gels (4–20% Mini-PROTEIN TGX™ Precast Gels) and electroblotted onto nitrocellulose membranes. The membranes were blocked (1 h) with Intercept blocking buffer from LI-COR (Cat. No. 927-60001, Lincoln, USA), incubated overnight with primary antibodies (1:1000 dilution), probed with near-infrared secondary antibodies (LI-COR) (1:5000 dilution), and visualized using an Odyssey imaging system (LI-COR, Lincoln, USA). Band intensities were quantified, and protein expression levels were analyzed relative to beta-actin.

EV isolation

After the overnight stimulation of hPAEpiC with the insults in T-150 flasks, 25 mL culture supernatant was collected in 50 mL Falcon™ tubes from Fischer Scientific (Cat. No. 14-959-49 A, Hampton, USA) and centrifuged at 2,000*g* for 10 min to remove cell debris. Supernatant was transferred into a fresh 50 mL tube and further centrifuged at 10,000*g* for 20 min to remove apoptotic bodies and other large particles from the media. The supernatant was further concentrated (5 mL–7.5 mL) using Amicon® Ultra-15 centrifugal filters from MilliporeSigma (Cat. No. UFC901024, Burlington, USA). Appropriate volume of ExoQuick-TC™ was added to the media (1 mL per 5 mL media), and the contents were mixed thoroughly by inverting the tubes, followed by overnight refrigeration at 4 °C. Next morning, contents were centrifuged at 2000*g* for 20 min at 4 °C, and the EV pellet was resuspended in sterile phosphate-buffered saline (PBS) without calcium and magnesium from MilliporeSigma (Cat. No. D8537, Burlington, USA).

Nanoparticle tracking analysis of EVs

The number and particle size distribution of hPAEpiC-EVs were analyzed by nanoparticle tracking analysis (NTA) using the NanoSight NS300 system (Malvern Technologies, Malvern, UK) fixed with a 488 nm laser. EV samples were diluted (1:500) in 1 mL particle-free MilliQ water (Milliporesigma, Burlington, USA) and injected into NanoSight chamber using 1 mL BD slip-tip syringe (Cat. No. 309659, Franklin Lakes, USA). Sample analysis was carried out under constant particle flow into the NanoSight chamber, and five 30-second videos were recorded for each sample. These videos record and track the path of unlabeled particles/EVs acting as point scatterers, undergoing Brownian motion in the chamber using laser beam [30]. Data collected in this fashion was later analyzed by NTA 3.3.104 software. Before running the samples, 100 nm latex beads from Malvern (Cat. No. NTA4088) were used to calibrate the system.

eATP detection in isolated EVs

hPAEpiC-EVs were resuspended in 150 μL PBS (Ca^{2+} and Mg^{2+} free) and lysed by ultrasonication at 4 °C. The EV suspension was centrifuged at 10,000*g* for 10 min, and 50 μL sample was loaded in duplicates in the Corning® black clear bottom 96-well plate (Cat. No. 3603, Corning, USA). Abcam luminescent ATP Detection assay kit (Cat. No. ab113849, Cambridge, UK) was used to measure eATP cargo in EVs by following the manufacturer's instructions.

DNA isolation from EVs

The EV suspension (100 μL) was treated with 10U of DNase from LGC Biosearch Technologies (Cat. No. DB0715K, Hoddesdon, UK) for 20 min at 37 °C to eliminate DNA attached to the EV surface. The DNase action was stopped by adding 10 μL 10X DNase stop solution at 65 °C for 10 min. EVs in suspension were further diluted by adding 100 μL nuclease-free water (NFW) and lysed by adding 20 μL proteinase K from Thermo Fisher (Cat. No. 4485229, Waltham, USA) at room temperature. After this step, the DNeasy® Blood & Tissue kit from Qiagen (Cat. No. 69506, Hilden, DE) was used to isolate DNA from EVs. We followed the manufacturer's instructions for DNA isolation, except for centrifugation at 20,000*g* for 1 min after the addition of AW2 buffer [31]. Similarly, spin columns were preincubated in AE buffer (30 μL) for 5 min before DNA elusion at room temperature. Remaining DNA in spin columns was also eluted by introducing an additional spin step. EV-DNA was quantified and stored at -20 °C prior to digital PCR (dPCR) assay.

mtDNA quantification by dPCR

A working concentration (1 ng/μL) of EV-DNA samples was prepared in NFW. Mitochondrial gene-specific Taqman™ probes for ATP8 [mt-ATP8] (Cat. No. 4331182 Hs02596863_g1), NADH dehydrogenase 2 [mt-ND2] (Cat. No. 4331182 Hs02596874_g1), and ferritin heavy chain 1 [mt-FTH1](Cat. No. 4331182 Hs02596865_g1) from Thermo Fisher Scientific (Waltham, USA) were used in dPCR experiments. For 10 μL dPCR reaction, we used 2 μL of 5X Absolute Q™ DNA Digital PCR Master Mix (Cat. No. A52490), 2 μL EV-DNA template (2 ng), 0.5 μL FAM-Taqman™ probe, and 5.5 μL NFW. Nine microliters of the above reaction mixture were loaded

onto QantStudio^{TM}MAP16 Digital PCR plate (Cat. No. 10246917). Lastly, 15 μL QuantStudio™ Isolation buffer (Cat. No. A52730) was added on top of each sample, and the wells were sealed with the gaskets supplied with the dPCR plates. The QuantStudio™ Absolute Q Digital PCR System from Thermo Fisher was used for DNA amplification, and QuantStudio dPCR software was used to count the number of microchambers with successful mtDNA amplification. The thermal profile of mtDNA dPCR was as follows: 10 min at 96 °C, followed by 40 cycles of 5 s at 96 °C and 15 s at 60 °C.

P2X7r ELISA

Cell culture supernatants collected from insult-stimulated hPAEpiC, with and without A80 treatment, were used to detect circulating P2X7r levels. Human purinergic P2RX7 ELISA Kit (Cat. No. RDR-P2RX7-Hu, Houston, USA) was used for this assay. In brief, 200 μL medium was added in appropriate wells, covered with a plate sealer, and incubated at 37 °C for 90 min. Culture media was removed from the wells and replaced with one hundred microliter detection solution 'A' followed by 45 min incubation at 37 °C. The wells were washed thrice with 300 μL 1X wash buffer. One hundred microliter detection solution 'B' was added to the wells and incubated at 37 °C for 45 min. The washing step was repeated as mentioned earlier, and 90 μL 'substrate solution' was added to the wells. The ELISA plate was incubated at 37 °C in the dark until a blue color developed in the wells (for 15–30 min). The enzymatic reaction was stopped by adding 50 μL stop solution. Absorbance was measured at 450 nm using a microplate reader (SpectraMax® M5).

Flow cytometry analysis of EVs

Magnetic streptavidin beads were conjugated with tetraspanin-coupled, biotinylated anti-CD9 or anti-CD63 antibodies provided in the Tetraspanin Exo-Flow Combo Capture Kit (System Biosciences, Palo Alto, USA). These magnetic beads were incubated with EV suspension overnight on a rotating mixer at 4 °C. During this step, EVs were captured on to the conjugated magnetic beads. The next morning, magnetic beads were washed thrice in 1X wash buffer to remove any unbound EV particles. EVs captured on to magnetic beads were resuspended in 500 μL wash buffer and incubated with 5 μg of anti-P2X7r antibody conjugated with Alexa Fluor™ 647 overnight on a rotating mixer at 4 °C. The magnetic beads were washed thoroughly to eliminate unbound P2X7r antibodies. EVs were stained with exo-FITC dye (System Biosciences). Cytometric acquisition was performed using an Aurora flow cytometer (Cytek®, San Diego, USA) and analyzed using FlowJo software v10 (Tree Star Inc., Ashland, USA) to check the distribution of P2X7r on EVs.

Intracellular Ca^{2+} analysis in hBMVECs after EV stimulation

Intracellular Ca^{2+} levels in hBMVECs were measured after overnight incubation with cell culture supernatant or EVs from hPAEpiC. Confluent hBMVECs cultured in their native growth media were stimulated with freshly collected hPAEpiC supernatant conditioned in ETH, ALD and e-Cig (1.8% or 0% nicotine), with and without A80 pre-treatment. hBMVECs incubated with fresh hPAEpiC-cultured media were used as media control. In another experiment, hBMVECs cultured in 12-well plate (4×10^5) were incubated with freshly isolated hPAEpiC-EVs (1:300). After 5 h incubation with EVs, intracellular Ca^{2+} levels in hBMVECs were measured using the calcium assay kit. Optimal condition for EV number and incubation time were determined from preliminary experiments (Supplementary Figure S2). During this experiment, hBMVECs were never exposed with either insults or A80 directly.

Results

P2X7r inhibition normalized mitochondrial oxidative phosphorylation (OXPHOS) in insult-exposed hPAEpiC

hPAEpiC exposed with ETH-, ALD-, and e-Cig (1.8% nicotine)-conditioned media increased the mito-stress levels in cells, resulting in reduced SRC levels as shown in line graph (Fig. 1A). Whereas, Fig. 1B-D illustrate 30–42% reduction in the SRC against ETH, ALD, and e-Cig (1.8% nicotine) exposure. Importantly, A80-pretreated hPAEpiC were protected from insult-driven mitochondrial stress, with restored SRC.

Increased P2X7r and TRPV1 channel expression led to Ca^{2+} accumulation in the insult-exposed hPAEpiC

After the overnight exposure of hPAEpiC to the insults, P2X7r and TRPV1 expression increased by 4–6-fold and 3–4-fold, respectively. A80 pretreatment significantly lowered the overexpression of both channels (Fig. 2A). e-Cig with 0% nicotine had no significant impact on the expression levels of P2X7r and TRPV1 channels. Furthermore, we found a 20-30-fold increase in intracellular Ca^{2+} accumulation in the insult-exposed hPAEpiC compared with untreated control cells. Interestingly, e-Cig with 0% nicotine also increased intracellular Ca^{2+} levels by 4-fold, which was a non-acute buildup and did not impact other functional readouts. A80 pretreatment significantly decreased the intracellular Ca^{2+} levels in the insult-exposed HPAEpiC (Fig. 2B).

Alteration in Ca^{2+} homeostasis upregulated the ER stress in the insult-exposed hPAEpiC

Transient stimulation of P2X7r and TRPV1 is known to facilitate Ca^{2+} influx into cells, stimulating diverse pro/anti-apoptotic pathways in a cell-specific manner [32,
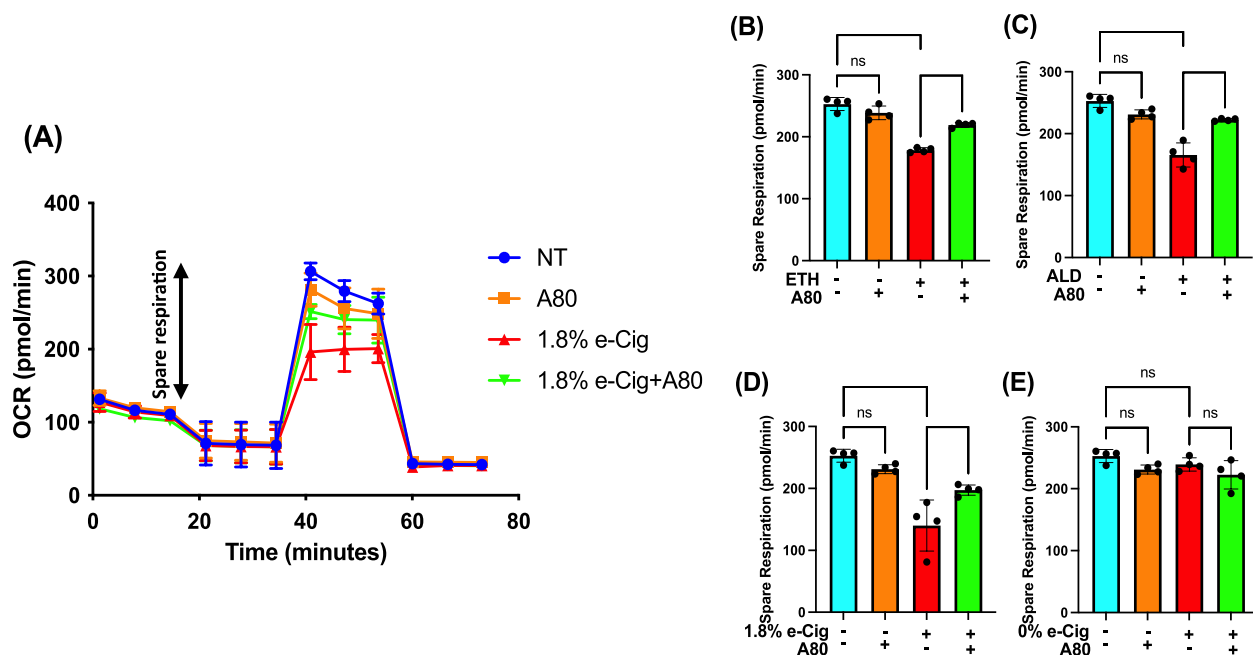
Fig. 1 P2X7r inhibition prevented mitochondrial dysfunction, induced by ETH, ALD, or e-Cig (1.8% nicotine). After overnight exposure to insults, mito-stress levels in hPAEpiC were measured using a Seahorse analyser, and the SRC were calculated. In figure, **A** line graph depicts the oxygen consumption rate (OCR), whereas Fig (**B**), (**C**), and (**D**) presents a 30%, 35%, and 42% reduction in spare respiration capacity (SRC) against 100 mM ETH, 100 μM ALD, and 1.75 μg/mL e-Cig (1.8% nicotine) stimulation, respectively. **E** e-Cig extract with 0% nicotine had no impact on mitochondrial spare respiration. In this figure, OCR represents the electron flow through the electron transport system linked to celluar ATP production and SRC was measured by subtracting the basal OCR from the maximal OCR. Pre-treatment with A80 (10 μM) restored OXPHOS levels in the insult-exposed hPAEpiC. Data were normalized to untreated control cells, and one-way ANOVA was used for statistical analyses, $*P \leq 0.05$, $****P \leq 0.0001$, and ns (not significant) where level of significance set at 0.05 ($n=4$)

33]. Unrestricted Ca^{2+} influx into the cytosol often interferes with ER Ca^{2+} levels, as most ER-localized chaperones depend on Ca^{2+} ions for their function. Disruption in ER Ca^{2+} levels causes protein aggregation, followed by unfolded protein response (UPR) [34]. The UPR promotes the phosphorylation of ER-specific, pro-apoptotic inositol-requiring enzyme 1 alpha (IRE1α) and its downstream regulator, apoptosis signal-regulating kinase (ASK1) MAP3K, forcing cells to undergo apoptosis [20, 35]. Using western blotting, we showed that hPAEpiC exposed with ETH-, ALD-, or e-Cig (1.8% nicotine)-conditioned media increased the phosphorylation of IRE1α and ASK1 by 2 to 3-fold, respectively. Simultaneously, the expression of anti-apoptotic protein Bax inhibitor-1 (BI-1) was down-regulated by 50%, potentially stimulating the apoptosis of hPAEpiC (Fig. 3). A80 pre-treatment reversed the expression level of ER stress markers in insult-exposed HPAEpiC.

Enhanced ER stress after ETH, ALD, or e-Cig (1.8% nicotine) stimulation increased lung epithelial EV numbers and particle-size

UPR stimulated by alcohol and other abusive drugs facilitates ER stress, followed by ER-Ca^{2+} efflux into the mitochondrial matrix, resulting in mitochondrial OXPHOS reduction and ROS accumulation [36, 37]. Mitochondrial dysfunction and ROS buildup promote EV release in mouse myeloblast cells [38]. Similarly, morphine-exposed BMVECs revealed redox imbalance, resulting in unwarranted EV release [39]. In this context, hPAEpiC exposed with ETH, ALD, and e-Cig (1.8% nicotine) conditioned media increased the EV release by 2 to 3 folds and average size of EVs were inflated by 20–30%. Pretreatment of hPAEpiC with A80 significantly reduced the EV number (Table 1). We further confirmed the tetraspanin profile (CD81 and CD9 expression) of isolated EVs by western blots (Fig. 4).

Larger EVs carried more eATP and mtDNA

Abusive drugs like cigarette smoke and alcohol are known to influence the EV cargo in liver and lung cells [40, 41]. In this direction, we measured eATP levels in isolated EVs after overnight stimulation of hPAEpiC with ETH-, ALD-, or e-Cig-conditioned media. ETH and ALD induced a 55-fold and 70-fold increase in eATP levels, respectively, while e-Cig (1.8% nicotine) stimulation resulted in a 110-fold increase. Although e-Cig (0% nicotine) stimulation increased the eATP levels in EVs, a
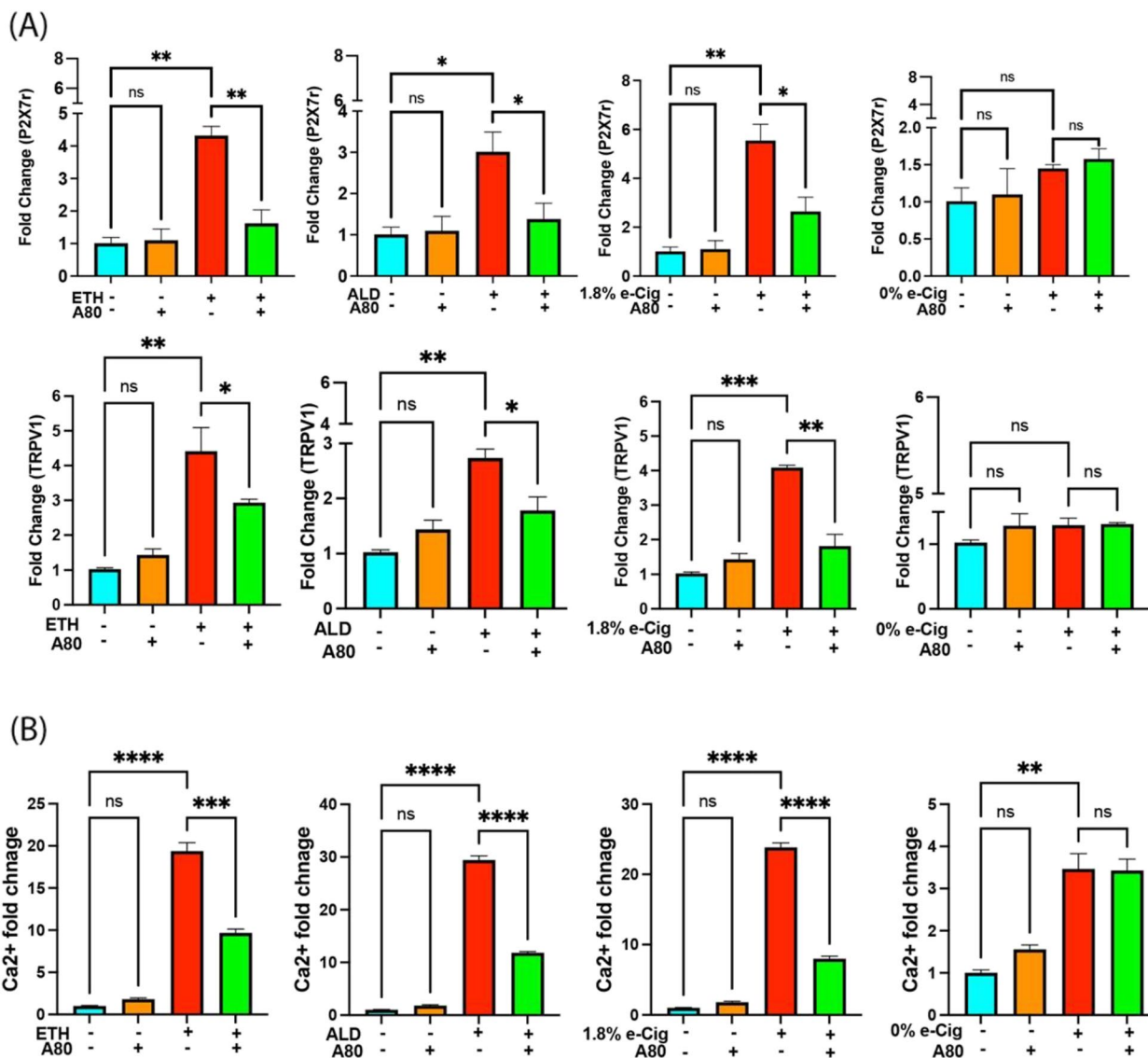
Fig. 2 ETH, ALD, and e-Cig (1.8% nicotine) increased P2X7r and TRPV1 expression and Ca^{2+} accumulation in hPAEpiC. **A** Overnight stimulation with ETH-, ALD-, and e-Cig (1.8% nicotine)-conditioned media increased P2X7r and TRPV1 gene expression by 4-6-fold and 3-4-fold, respectively. A80 pretreatment significantly lowered the P2X7r and TRPV1 expression in cells. e-Cig (0% nicotine)-conditioned media had no significant effect on P2X7r and TRPV1 expression in hPAEpiC. qPCR data were normalized to untreated cells, and GAPDH was used as a housekeeping gene. **B** Inhibition of P2X7r and TRPV1 expression by A80 reduced Ca^{2+} accumulation in insult-treated hPAEpiC. Overnight stimulation with ETH-, ALD-, and e-cig (1.8% nicotine)-conditioned media increased intracellular Ca^{2+} levels by 20-30-folds. A80 pretreatment significantly reduced the levels. Data were normalized with untreated control cells. One-way ANOVA was used for statistical analyses. *$P \leq 0.05$, **$P \leq 0.01$, ***$P \leq 0.001$, ****$P \leq 0.0001$, and ns (not significant) ($n = 3$)

(See figure on next page.)
Fig. 3 P2X7r inhibition prevented ER stress that was escalated by ETH, ALD, or e-Cig (1.8% nicotine) in hPAEpiC. **A** Representative western blot image from one of three independent experiments. **B** Bar graphs show 2 to 3-fold increase in the expression of the ER stress markers IRE1α and pASK1, while the expression of the antiapoptotic Bax inhibitor-1 (BI-1) protein was cutdown by 50%, resulting in the amplification of mito-stress levels in hPAEpiC. A80 diminished pro-apoptotic protein expression and restored antiapoptotic protein expression. Western blot data were normalized to β-actin. One-way ANOVA was used for statistical analyses, *$P \leq 0.05$, **$P \leq 0.01$, ***$P \leq 0.001$, and ns (not significant) ($n = 3$)
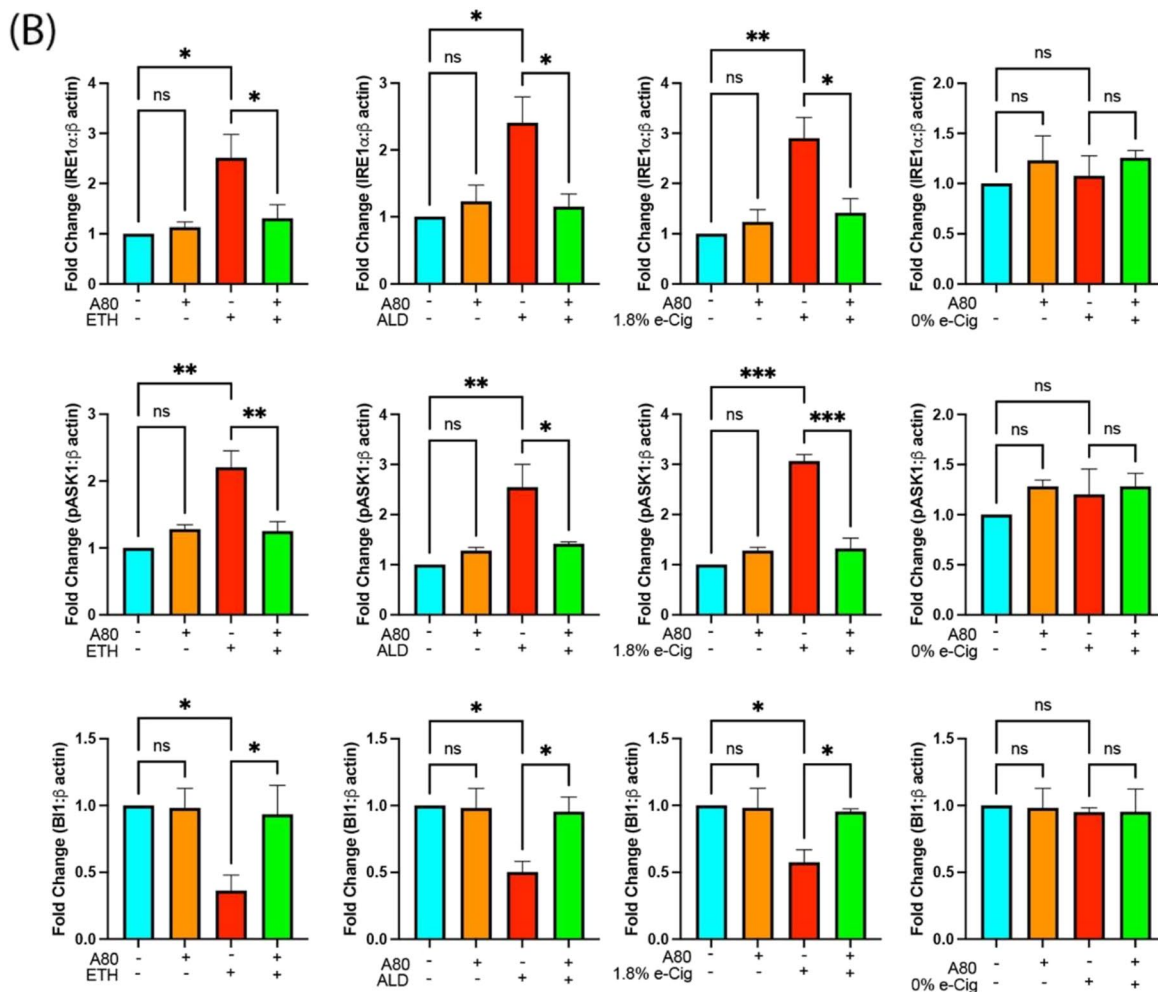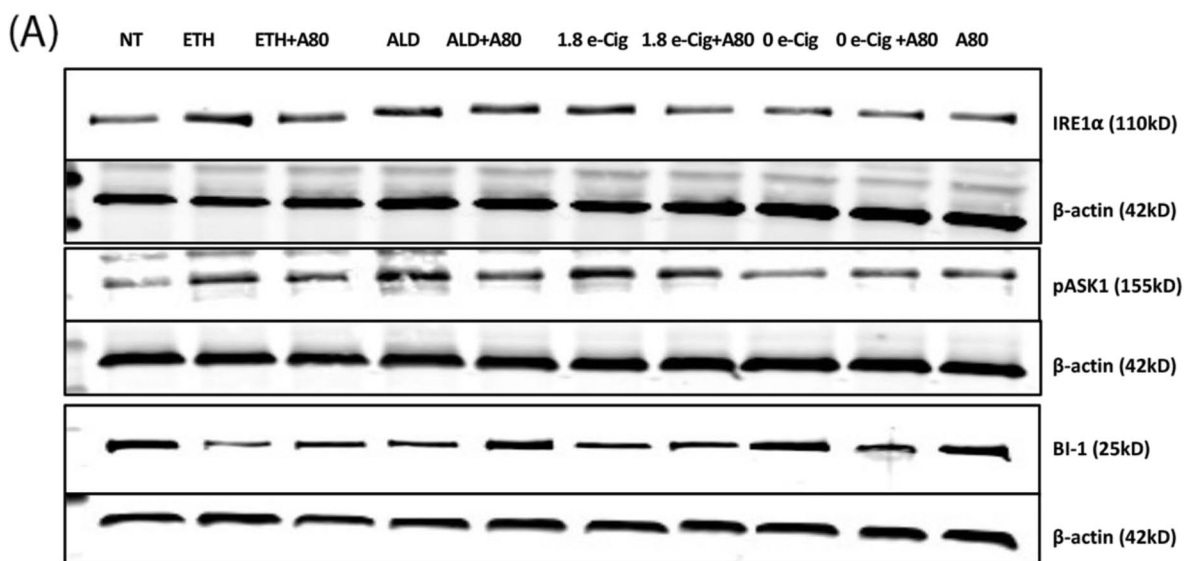
Fig. 3 (See legend on previous page.)

Mekala *et al. Cell Communication and Signaling*   (2024) 22:39

Page 9 of 16

Table 1 ETH, ALD, and e-Cig (1.8% nicotine) exposure increased the size and numbers of shed lung epithelial EVs, and P2X7r inhibition brought them to control levels

S.No	Treatment	Particle size ± standard error	Concentration (particles/mL)
1	Nontreated (NT)	136.8 ± 4.7 nm	3.04×10^8
2	ETH	149.5 ± 4.4 nm	6.11×10^8
3	ETH + A80	127.2 ± 5.7 nm	4.88×10^8
4	ALD	155.3 ± 3.5 nm	8.71×10^8
5	ALD + A80	126.7 ± 3.6 nm	6.11×10^8
6	1.8% e-Cig	153.8 ± 6.8 nm	8.10×10^8
7	1.8% e-Cig + A80	138.7 ± 2.5 nm	6.08×10^8
8	0% e-Cig	145.8 ± 5.6 nm	4.16×10^8
9	0% e-Cig + A80	138.9 ± 5.4 nm	3.85×10^8
10	A80	134.0 ± 4.3 nm	4.01×10^8

(A) Overnight stimulation of hPAEpiC with ETH, ALD, and e-Cig (1.8% nicotine)-conditioned media increased the EV particle size by 20–30%. The EV number was increased by 2-fold after ETH exposure and 3-fold after ALD or e-Cig (1.8% nicotine) exposure. In contrast, A80 pretreatment decreased the size and number of EVs. Data is presented as mode ± standard error ($n = 3$)

2-fold change was insufficient to influence downstream events. Simultaneous pretreatment with A80 significantly lowered eATP levels in hPAEpiC-EVs (Fig. 5A).

We used high-throughput dPCR to measure the absolute copy numbers of mtDNA in the EVs using Taqman™ probes targeting various segments of the mtDNA. Overnight stimulation with ETH-, ALD-, or e-Cig (1.8% nicotine)-conditioned media increased the copies of mt-ATP8, mt-ND2, and mt-FTH1 in the EVs by 2-fold, whereas pretreatment with A80 effectively diminished the mtDNA cargo (except mt-FTH1 levels after ETH stimulation) (Fig. 5B). e-Cig (0% nicotine) did not show significant changes in the mtDNA levels when compared to the untreated control group. We presented dPCR data in fold change to show statistical significance between experimental replicates.

ETH, ALD, or e-Cig (1.8% nicotine) exposure promoted P2X7r shedding via cell supernantant and EVs

In hPAEpiC supernatant, ETH and e-Cig (1.8% nicotine) stimulations elevated the P2X7r levels by 6-fold. ALD

exposure led to an 8-fold increase in P2X7r levels. Cell supernatant from A80-pretreated cells had significantly lower P2X7r levels compared to insult-exposed cells. e-Cig (0% nicotine) had no effect on P2X7r shedding (Fig. 6A).

Flow cytometric analysis of EVs was performed to assess the potential distribution of P2X7r on the EV surface. ETH, ALD, and e-Cig (1.8% nicotine) stimulations increased median fluorescence intensity (MFI) by 50 to 60%, showing greater P2X7r cargo on the EVs compared with the EVs from the unexposed-cells. EVs isolated from A80-pretreated, insult-exposed cells showed lower P2X7r MFI than only insult-exposed cells. E-Cig (0% nicotine) stimulation showed no effects on MFI (Fig. 6B).

Soluble P2X7r and eATP released from hPAEpiC-EVs induce paracrine signaling in BMVECs

Extracellular ATP-gated P2X7r activation stimulates Ca^{2+} influx into the cytosol, activating inflammasome assembly and caspase-1 [42]. Recently, circulating P2X7r was shown to trigger inflammasome formation in the brain of epilepsy patients [43]. In our studies, we examined the paracrine signaling between hPAEpiC and human BMVECs by culturing BMVECs in hPAEpiC-conditioned media. After overnight stimulation, intracellular Ca^{2+} levels were measured in BMVECs. Media from ETH-exposed hPAEpiC increased the BMVEC's Ca^{2+} levels by 2-fold, whereas ALD or e-Cig (1.8% nicotine)-conditioned media escalated the BMVEC's Ca^{2+} levels by 4-fold. Media preconditioned with A80 had considerably reduced intracellular Ca^{2+} levels in BMVECs (Fig. 7A). BMVECs incubated in media from unexposed-hPAEpiC were used as a media control.

To prove the specific effects of the signaling abilities of lung EVs, we incubated BMVECs with freshly isolated lung EVs (300 EVs/cell). After 5 h incubation, intracellular Ca^{2+} levels were measured using a calcium assay. EVs isolated after ETH, ALD, and e-Cig (1.8% nicotine) stimulation amplified the intracellular Ca^{2+} levels by 2-3-fold, whereas EVs from A80-pretreated cells presented lower Ca^{2+} levels (Fig. 7B). Of note, recombinant P2X7r (used as a control) also increased Ca2+accumulation in
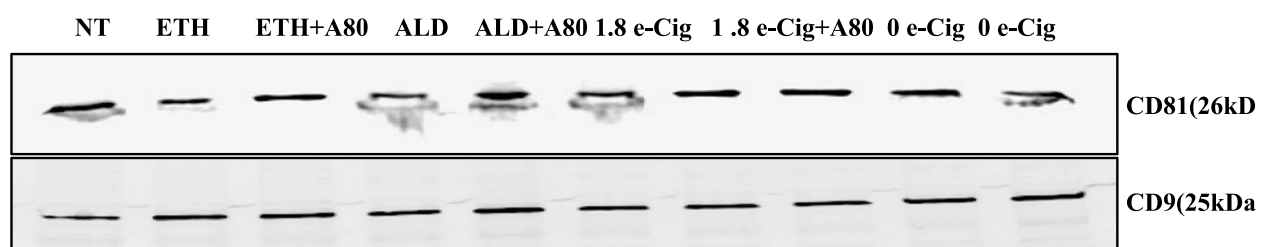

Fig. 4 EVs were further evaluated for the presence of CD81 and CD9 markers using western blot

Mekala *et al. Cell Communication and Signaling*   (2024) 22:39
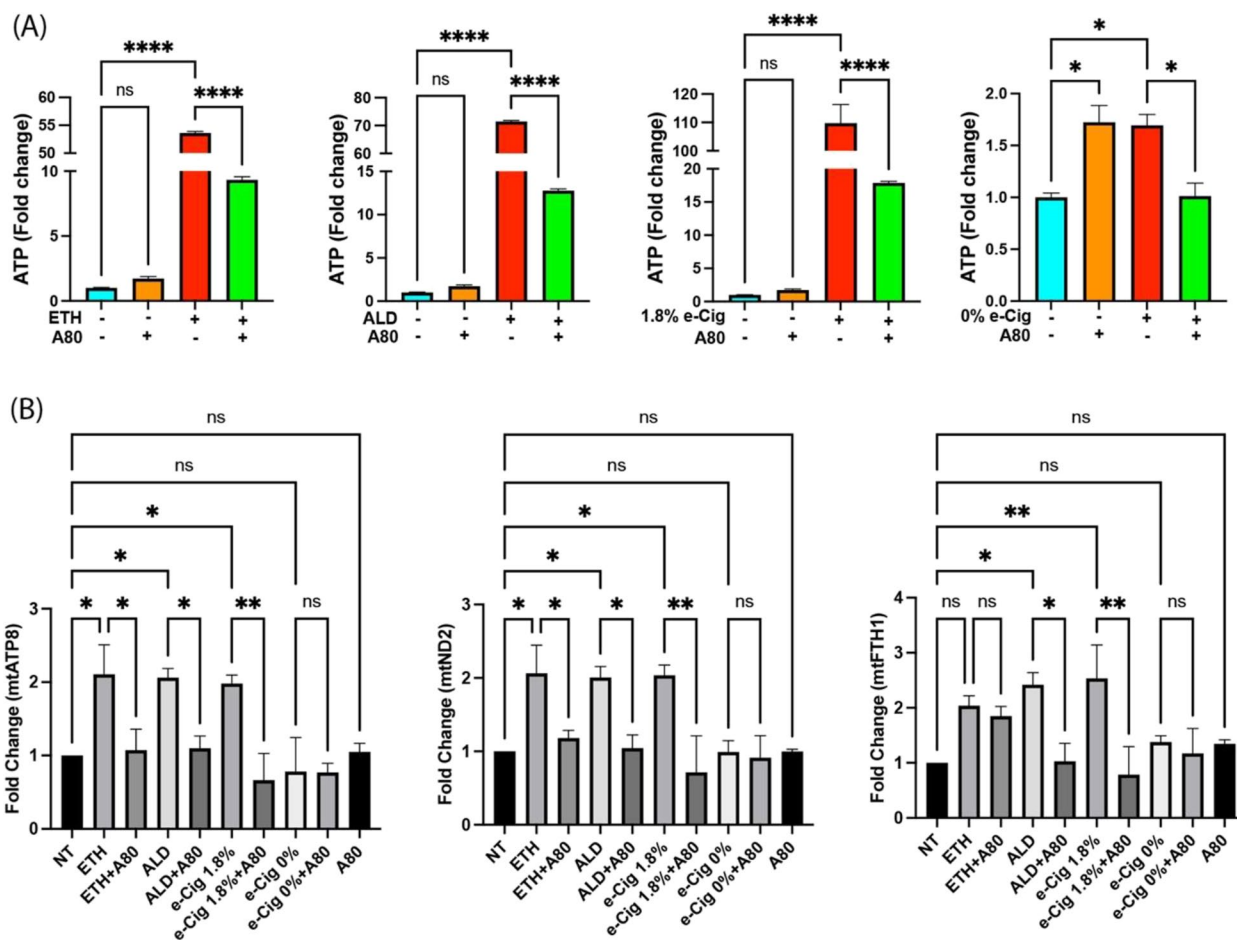
Page 10 of 16

Fig. 5 ETH, ALD, or e-Cig (1.8% nicotine) stimulation facilitated eATP and mtDNA buildup in hPAEpiC-EVs. **A** In isolated EVs, both ETH and ALD stimulation increased the eATP levels by 55-fold and 70-fold, respectively, whereas e-Cig (1.8% nicotine) stimulation elevated the eATP levels by 110-fold. EVs isolated from hPAEpiC pretreated with A80 showed significantly lower eATP levels. Although, eATP levels in e-Cig (0% nicotine)-treated cells are significant, fold changes were small compared to other insults. **B** dPCR was used to quantify the copy numbers of mtDNA present in EVs, and bar graphs represent the fold changes in the experimental groups, normalized to EVs from untreated control. We used 2 ng of EV DNA for dPCR amplification. Overnight stimulation with ETH, ALD, and e-Cig (1.8% nicotine) doubled the mtDNA cargo, whereas A80 pretreatment could successfully block the mtDNA assembly in EVs. One-way ANOVA was used for statistical analyses, $*P \leq 0.05$, $**P \leq 0.001$, $****P \leq 0.0001$, and ns (not significant) ($n = 3$)

BMVECs, establishing the functional role of P2X7r as a Ca2+channel.

Discussion

In this report, we studied the harmful effects of alcohol, e-Cig vaping, and their byproducts on mitochondrial homeostasis in hPAEpiC, EV shedding, and EV cargo content. In mitochondria, respiratory capacity depends on the efficiency of electron transport complexes and mitochondrial membrane potential [44]. In the liver, chronic alcohol consumption and cigarette smoke accelerate reactive oxygen and nitrogen species (ROS/RNS) accumulation through NADPH oxidase (NOX) and cytochrome P450-2E1 (CYP2E1) enzyme activation [45].

In an intracerebral hemorrhage mouse model, P2X7r activation is shown to mediate NOX-dependent ROS production, followed by mitochondrial degradation [46]. NOX is a catalytic enzyme that transfers electrons (e^-) from NADPH to oxygen, generating superoxide radicals ($O_2^{\bullet-}$) [47]. CYP2E1 is an ethanol-catabolizing enzyme, known for ROS/RNS generation in significant amount [48]. Upon ROS/RNS buildup, the inner mitochondrial membrane quickly depolarizes and limits the OXPHOS levels [49]. In our Seahorse experiments, hPAEpiC exposed with ETH-, ALD-, or e-Cig-conditioned media significantly reduced the OXPHOS levels, confirming the detrimental effects of abusive drugs on mitochondrial function (Fig. 1). Also, P2X7r inhibition restored
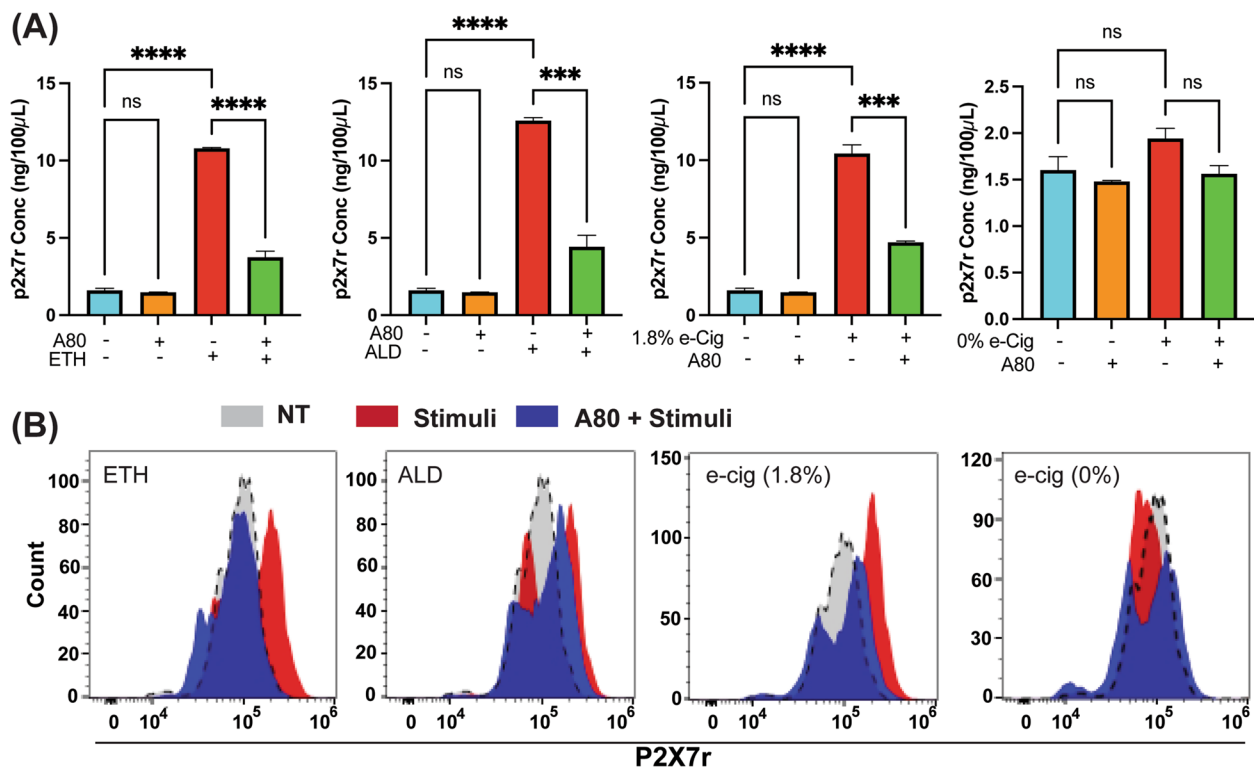
(A)

(B)

NT   Stimuli   A80 + Stimuli

P2X7r

Fig. 6 ETH, ALD, or e-Cig (1.8% nicotine) exposure increased the circulating P2X7r levels both in culture supernatant and on the EV surface. **A** ETH or e-Cig (1.8% nicotine) stimulation resulted in a 6-fold increase in circulating P2X7r levels, and ALD stimulation elevated circulating/soluble P2X7r level by 8-fold. Media from A80 pretreated, insult-exposed cells showed significantly lower P2X7r levels than media with only insult-exposed cells. One-way ANOVA was used for statistical analyses; ***$P \leq 0.001$ ****$P \leq 0.0001$, and ns (not significant) ($n = 3$). **B** EVs captured on to the magnetic beads presented increased MFI values (P2X7r distribution) after ETH (1.6-fold), ALD (1.5-fold), and 1.8% e-Cig stimulation (1.53-fold), and pretreatment with P2X7r antagonist (A80) successfully reduced the MFI values

the mitochondrial OXPHOS levels, confirming the role of P2X7r in regulating mitochondrial health in hPAEpiC.

P2X receptors are a family of ligand-gated ion channels, gated by eATP, and exist in seven isoforms, P2X1 to P2X7 receptors [50]. Unlike other P2X receptors, P2X7r needs excess ATP for its activation (three ATP molecules for one P2X7r). Activated P2X7r known to regulate Ca^{2+} and sodium (Na^+) influx and potassium (K^+) efflux in cells [51], mediate actin and tubulin rearrangement [52], promote inflammation [53], and encourages mitochondrial swelling/rupture to release pro-apoptotic cytochrome C into the cytosol [54]. While the involvement of P2X7r in various pathophysiological conditions is well reported, its potential role in substance abuse attracted attention only recently [55, 56]. Similarly, TRPV1 is a highly selective Ca^{2+} channel, which facilitates cigarette smoke-associated airway inflammation [57] and opioid-induced hyperglycemia [58]. In our studies, ETH, ALD, and e-Cig (1.8% nicotine) stimulation increased the gene expression of both P2X7r and TRPV1, enhancing Ca^{2+} influx into the hPAEpiC (Fig. 2). Such a sudden increase

in intracellular Ca^{2+} levels can promote cytoskeletal remodeling [59], alter Ca^{2+} levels in the ER lumen, and activate Ca^{2+}-dependent ER stress, leading to cell death [20]. As expected, the P2X7r inhibitor A80 successfully curbed the P2X7r and TRPV1 overexpression and reduced the Ca^{2+} influx into the hPAEpiC.

ER stores the large amount of Ca^{2+} with a steep concentration gradient between the ER (up to 1 mM) and cytosol (approximately 100 nM) [60]. ER-Ca^{2+} levels are vital for the post-translational modifications of transmembrane proteins in the ER lumen [34]. Cytosolic Ca^{2+} acts as an intracellular messenger that controls diverse cellular functions, and any disruption in cytosolic Ca^{2+} homeostasis can be toxic and cause cell death [61]. In our experiments, the P2X7r and TRPV1 overexpression significantly increased the intracellular Ca^{2+} levels in hPAEpiC, exposed to ETH, ALD, or e-Cig (1.8% nicotine). Under these pathological conditions, excess Ca^{2+} can be shuttled and stored in the ER by the energy-consuming sarcoplasmic/endoplasmic reticulum calcium ATPase (SERCA2b) [62]. SERCA2b overexpression during chronic inflammation promotes dramatic Ca^{2+}
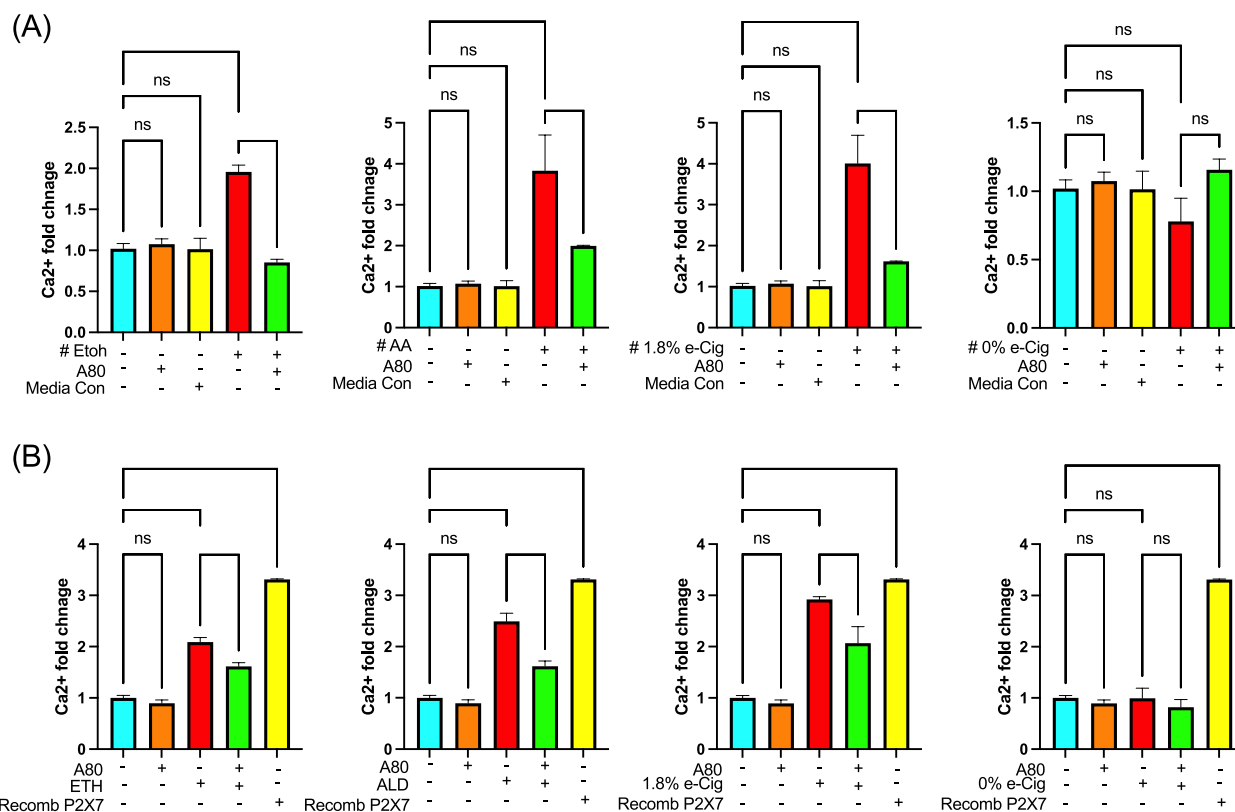
Fig. 7 Circulating P2X7r and eATP mediated intercellular signaling between hPAEpiC and hBMVECs. **A** Conditioned epithelial cell culture media with ETH induced a 2-fold increase in Ca^{2+} levels in BMVECs, and 4-fold increase against ALD or e-Cig (1.8% nicotine) conditioned media. BMVECs treated with media preconditioned with A80 could successfully block the intracellular Ca^{2+} accumulation. BMVECs incubated with lung epithelial cell media were used as a media control. **B** Lung epithelial EVs shed against ETH, ALD, and e-Cig (1.8% nicotine) stimulation were incubated (5 h) with BMVECs (300 EVs/cell). Lung EVs increased the BMVEC's Ca^{2+} levels 2 to 3-fold. Human recombinant P2X7r protein expressed in the prokaryotic system (500ng/ml) from LS bio was used as a positive control. One-way ANOVA was used for statistical analyses, *$P \le 0.05$, **$P \le 0.01$, ***$P \le 0.001$, ****$P \le 0.0001$, and ns (not significant) ($n = 3$)

uptake by the ER, resulting in increased UPR in the ER [63].

IRE1α is an evolutionarily conserved ER membrane protein involved in the regulation of both cell survival and death mechanisms [64]. As discussed earlier, most secretory proteins are produced in the ER lumen and ER-Ca^{2+} levels are vital for proper protein folding [65]. Any fluctuations in ER-Ca^{2+} levels lead to protein misfolding, followed by UPR, which serve as direct ligands for IRE1α activation [66]. Its prolonged activation triggers the apoptosis-inducing molecule, tumor necrosis factor receptor-associated factor 2 (TRAF2), through its cytosolic domain. This further activates its downstream pASK1, a MAP kinase kinase kinase (MAP3K), which later phosphorylates c-Jun N-terminal kinase and p38, leading to apoptotic cell death [67, 68]. On the contrary, BI-1 plays a protective role against ER-Ca^{2+} buildup. BI-1 facilitates Ca^{2+} flow from the ER into the mitochondrial matrix via the mitochondrial permeability transition pore, thereby restoring Ca^{2+} levels in the ER lumen [69,

70]. In the present study, Ca^{2+} influx triggered by ETH, ALD, or e-Cig stimulation increased the expression of IRE1α and pASK1proteins, leading hPAEpiC to undergo severe stress. By lowering BI-1 protein expression, ETH, ALD, or e-Cig (1.8% nicotine) stimulation promoted toxic ER-Ca^{2+} levels (Fig. 3). P2X7r inhibition by A80 restored the ER-Ca^{2+} levels and reduced the expression of IRE1α and pASK1proteins, ensuring lung epithelial cell survival.

EVs released from injured cells differ significantly in their structure and function. EVs carry and transport unique biomolecules depending on the disease conditions, making them perfect biomarkers [71]. In lung carcinoma cells, nicotine stimulation increases EV number and transforms EVs' morphology with an altered miRNA profile [72]. Active inhalation of nicotine-containing e-Cig vape increased circulating EV number, shed by endothelial cells and loaded with proinflammatory CD40 markers [73]. In patients, nicotine consumption aggravates the spread of atherosclerotic lesions, potentially via EVs containing miR-21-3p cargo [74]. Likewise,

liver injury inflicted by alcohol abuse also exaggerates EV release, carrying inflammatory signaling molecules (NFκB, TLR4, IL-1 receptors, caspase-1) into the circulation [75]. In the brain, cocaine-induced oxidative stress weakens mitochondrial membrane potential, forcing the mitochondria to rupture and release their contents via EVs [76, 77].

P2X7r activation by eATP and/or NAD+molecules promotes P38-MAPK-facilitated cytoskeletal restructuring in macrophages, resulting in EV release [78]. However, under normal conditions, intercellular ATP and NAD$^+$ levels remain low for P2X7r activation. Chronic alcohol exposure in humans stimulates inflammasome activation in the liver and brain, followed by tissue damage, resulting in substantial eATP release [79]. Once released, eATP acts as an endogenous mediator and enhances EV release [80, 81]. eATP that are endocytosed into EVs also mediate actin rearrangement and influence EV size, shape, and adhesion properties [82]. According to our NTA data, hPAEpiC stimulated with ETH-, ALD-, or e-Cig (1.8% nicotine)-conditioned media, generated more EVs (2-fold to 3-fold increase) with larger size than unexposed hPAEpiC (Fig. 4). Pretreatment with A80 reverted the EV numbers and size to those shed by untreated hPAEpiC.

In the mouse brain, cocaine-induced inflammation promotes the release of small EVs (exosomes) loaded with mtDAMPs, including misfolded mito-proteins, eATP, ROS, and degraded mtDNA [83]. When released, these mtDAMPs can activate numerous proinflammatory autocrine and paracrine signaling in recipient cells, producing several inflammation-associated diseases [84]. In our studies ETH, ALD, or e-Cig (1.8% nicotine) exposure increased eATP cargo in EVs. dPCR analyses showed the large quantities of mtDNA embedded in the lung epithelial EVs (Fig. 5), which can act as mtDAMPs. P2X7r inhibition in lung cells exposed with ETH-, ALD-, or e-Cig-conditioned media reversed EV cargo, confirming the role of the P2X7r pathway on lung-EV release and on its cargo.

In addition to their unique cargo-carrying capacity, EVs also carry surface ligands/receptors, allowing EVs to target other cells [85]. Once attached on the recipient cell, EVs transmit signals via receptor-ligand interaction or internalized by endocytosis or fused with the recipient cell membrane, delivering their cargo into its cytosol, thereby altering the functional state of the recipient cell [86]. In human macrophages, P2X7r stimulation by eATP promotes inflammation and release of EVs loaded with IL-1b and P2X7r [87, 88]. Similarly, chronic inflammatory responses seen in diabetic and COVID19 patients resulted in P2X7r release into the circulation [89, 90], most likely through EVs. Our studies demonstrated

significant quantities of circulating P2X7r in the lung epithelial cell media and EVs with greater P2X7r expression on their surface (Fig. 6) against ETH, ALD, or e-Cig (1.8% nicotine) stimulation. P2X7r can further stimulate inflammation in recipient cells directed by NLRP3 activation [91].

Interestingly, we detected a variety of cargoes (eATP, mtDNA) in hPAEpiC-EVs that can act as mtDAMPs, which can trigger NLRP3 inflammasome mediated BBB damage [92, 93]. P2X7r found on EVs is known to activate NLRP3-mediated Ca^{2+} accumulation in bone marrow cells [94]. In this cotext, we assessed the paracrine signaling efficacy of biomolecules detected in lung EVs by incubating BMVECs (cells constituting BBB) with lung epithelial cell-spent media and freshly isolated lung EVs. In both experiments, in line with circulating eATP (Fig. 5) and P2X7r levels (Fig. 6), we noticed a significant amount of Ca^{2+} accumulation in hBMVECs (Fig. 7), whereas spent media and EVs derived from epithelial cells pretreated with A80 displayed lower Ca^{2+} levels, endorsing the paracrine signaling induced by alcohol or nicotine-containing e-Cig in hPAEpiC and BMVECs. Notably, recombinant P2X7r added to hBMVECs resulted in the similar functional changes as ETH, ALD, or e-Cig (1.8% nicotine) executed (Fig. 7B).

In all our experiments, we exposed hPAEpiC with e-Cig (0% nicotine)-conditioned media, as our earlier studies with nicotine-free e-Cig vape produced pathological effects on mouse brain and lung tissues [3]. Airway epithelail cells exposed with nicotine-free e-Cig vape also increased the IL-6 levels [95] and limited the oxygen levels in circulation [96]. Some studies in patients with asthma have also shown that nicotine-free e-liquids, made of high grade, contaminant-free mixture of propylene glycol and glycerol, did not impact lung function [97]. In this report, nicotine-free e-Cig media increased P2X7r levels marginally, resulting in a partial increase in intracellular Ca^{2+} levels, which did not affect any of our functional assays.

Conclusion
The current study demonstrated the harmful effects of e-Cig (1.8% nicotine), ETH, and its main metabolite ALD on mitochondrial function in hPAEpiC, which form an alveolar barrier. Ca^{2+} accumulation promoted by drugs of abuse stimulates ER stress, increase EV release bolstering greater eATP, P2X7r cargo transport. Mito-stress induced by ETH and e-Cig (1.8% nicotine) stimulation induce the mitochondrial membrane damage, letting mtDNA escape through EVs. A variety of cargo detected in hPAEpiC-EVs act as potential stimulants of inflammation and trigger functional changes in BMVECs, indicative of BBB injury. These observations

Mekala *et al. Cell Communication and Signaling*   (2024) 22:39

Page 14 of 16

also demonstrate the mechanisms of distant organ injury by e-Cig or alcohol. Similar functional changes exerted by recombinant P2X7r in BMVECs, confirms its role as a paracrine signaling molecule for the first time. Inhibition of P2X7r diminished all pathological effects caused by ETH, ADH or e-Cig (1.8% nicotine) in hPAEpiC. We will continue to test the impacts of abusive drugs on P2X7r expression and its extracellular sheding in the mouse model and test P2X7r paracrine siganling in the BBB damage.

Abbreviations

ETH	Ethanol
ALD	Aldehyde
e-Cig	Electronic cigarette
hPAEpiC	Human pulmonary alveolar epithelial cells
hBMVECs	Human brain microvascular endothelial cells
mtDNA	Mitochondrial DNA
eATP	Extracellular ATP
NLRP3	NLR family pyrin domain containing 3
P2X7r	P2X purinergic receptor 7
TRPV1	Transient receptor potential vanilloid 1
FCCP	Carbonyl cyanide p-trifluoro methoxyphenylhydrazone
OXPHOS	Oxidative phosphorylation
SRC	Spare respiratory capacity
ROS	Reactive oxygen species
RNS	Reactive nitrogen species
ER	Endoplasmic reticulum
UPR	Unfolded protein response
mtDAMPs	Mitochondrial damage-associated molecular patterns

Supplementary Information

The online version contains supplementary material available at https://doi.org/10.1186/s12964-023-01461-1.

Additional file 1.

Additional file 2.

Additional file 3.

Authors' contributions

Conceptualization, N.M. and Y.P.; Methodology, N.M., J.T. and N.T.; Validation, N.M. and N.T.; Formal Analysis, N.M. and S.R.; Investigation, N.M. and S.R.; Resources, Y.P.; Writing – Original Draft Preparation, N.M.; Writing – Review & Editing, U.S., P.B. and Y.P.; Supervision, Y.P.; Funding Acquisition, Y.P.

Funding

Availability of data and materials

Not applicable.

Declarations

Competing interests

The authors declare no competing interests.

Author details

[1]Department of Pathology and Laboratory Medicine, Lewis Katz School of Medicine, Temple University, Philadelphia, PA 19140, USA.

References

1. Jones K, Salzman GA. The Vaping Epidemic in adolescents. Mo Med. 2020;117(1):56–8.
2. Morean ME, Bold KW, Kong G, Gueorguieva R, Camenga DR, Simon P, Jackson A, Cavallo DA, Krishnan-Sarin S. Adolescents' awareness of the nicotine strength and e-cigarette status of JUUL e-cigarettes. Drug Alcohol Depend. 2019;204:107512.
3. Heldt NA, Seliga A, Winfield M, Gajghate S, Reichenbach N, Yu X, Rom S, Tenneti A, May D, Gregory BD, et al. Electronic cigarette exposure disrupts blood-brain barrier integrity and promotes neuroinflammation. Brain Behav Immun. 2020;88:363–80.
4. Wetherill RR, Doot RK, Young AJ, Lee H, Schubert EK, Wiers CE, Leone FT, Mach RH, Kranzler HR, Dubroff JG. Molecular imaging of pulmonary inflammation in users of electronic and combustible cigarettes: a pilot study. J Nucl Med. 2023;64(5):797–802.
5. Scott A, Lugg ST, Aldridge K, Lewis KE, Bowden A, Mahida RY, Grudzinska FS, Dosanjh D, Parekh D, Foronjy R, et al. Pro-inflammatory effects of e-cigarette vapour condensate on human alveolar macrophages. Thorax. 2018;73(12):1161–9.
6. Clapp PW, Lavrich KS, van Heusden CA, Lazarowski ER, Carson JL, Jaspers I. Cinnamaldehyde in flavored e-cigarette liquids temporarily suppresses bronchial epithelial cell ciliary motility by dysregulation of mitochondrial function. Am J Physiol Lung Cell Mol Physiol. 2019;316(3):L470–86.
7. Poole LG, Beier JI, Torres-Gonzales E, Schlueter CF, Hudson SV, Artis A, Warner NL, Nguyen-Ho CT, Dolin CE, Ritzenthaler JD, et al. Chronic + binge alcohol exposure promotes inflammation and alters airway mechanics in the lung. Alcohol. 2019;80:53–63.
8. Appolonia CN, Wolf KM, Zawatsky CN, Cinar R. Chronic and binge alcohol ingestion increases truncated oxidized phosphatidylcholines in mice lungs due to increased oxidative stress. Front Physiol. 2022;13:860449.
9. Samokhvalov AV, Irving HM, Rehm J. Alcohol consumption as a risk factor for pneumonia: a systematic review and meta-analysis. Epidemiol Infect. 2010;138(12):1789–95.
10. Hulsebus HJ, Najarro KM, McMahan RH, Boe DM, Orlicky DJ, Kovacs EJ. Ethanol intoxication impairs respiratory function and bacterial clearance and is Associated with Neutrophil Accumulation in the lung after Streptococcus pneumoniae infection. Front Immunol. 2022;13:884719.
11. Robin MA, Sauvage I, Grandperret T, Descatoire V, Pessayre D, Fromenty B. Ethanol increases mitochondrial cytochrome P450 2E1 in mouse liver and rat hepatocytes. FEBS Lett. 2005;579(30):6895–902.
12. Manzo-Avalos S, Saavedra-Molina A. Cellular and mitochondrial effects of alcohol consumption. Int J Environ Res Public Health. 2010;7(12):4281–304.
13. Hirano T, Kaplowitz N, Tsukamoto H, Kamimura S, Fernandez-Checa JC. Hepatic mitochondrial glutathione depletion and progression of experimental alcoholic liver disease in rats. Hepatology. 1992;16(6):1423–7.
14. Valavanidis A, Vlachogianni T, Fiotakis K, Loridas S. Pulmonary oxidative stress, inflammation and cancer: respirable particulate matter, fibrous dusts and ozone as major causes of lung carcinogenesis through reactive oxygen species mechanisms. Int J Environ Res Public Health. 2013;10(9):3886–907.
15. Gicquel T, Victoni T, Fautrel A, Robert S, Gleonnec F, Guezingar M, Couillin I, Catros V, Boichot E, Lagente V. Involvement of purinergic receptors and NOD-like receptor-family protein 3-inflammasome pathway in the adenosine triphosphate-induced cytokine release from macrophages. Clin Exp Pharmacol Physiol. 2014;41(4):279–86.
16. Cicko S, Kohler TC, Ayata CK, Muller T, Ehrat N, Meyer A, Hossfeld M, Zech A, Di Virgilio F, Idzko M. Extracellular ATP is a danger signal activating P2X7 receptor in a LPS mediated inflammation (ARDS/ALI). Oncotarget. 2018;9(55):30635–48.
17. Santiago-Carvalho I, de Almeida-Santos G, Bomfim CCB, de Souza PC, Silva J, de Melo BMS, Amaral EP, Cione MVP, Lasunskaia E, Hirata MH, et al. P2x7 Receptor Signaling Blockade Reduces Lung Inflammation and Necrosis During Severe Experimental Tuberculosis. Front Cell Infect Microbiol. 2021;11:672472.
18. Chipurupalli S, Samavedam U, Robinson N. Crosstalk between ER stress, autophagy and inflammation. Front Med (Lausanne). 2021;8:758311.
19. Shen L, Wang Z, Wang R, Chen X, Cheng S. Upregulation of the P2X7 receptor promotes Ca(2+) accumulation and inflammatory response in post-stroke depression. Am J Transl Res. 2021;13(9):10276–87.

20. Mekala N, Gheewala N, Rom S, Sriram U, Persidsky Y. Blocking of P2X7r reduces mitochondrial stress Induced by Alcohol and electronic cigarette exposure in Brain Microvascular endothelial cells. Antioxidants. 2022;11(7):1328.

21. Golia MT, Gabrielli M, Verderio C. P2X(7) receptor and Extracellular Vesicle Release. Int J Mol Sci. 2023;24(12):9805.

22. Joshi BS, de Beer MA, Giepmans BNG, Zuhorn IS. Endocytosis of Extracellular vesicles and release of their Cargo from endosomes. ACS Nano. 2020;14(4):4444–55.

23. Anand S, Samuel M, Kumar S, Mathivanan S. Ticket to a bubble ride: Cargo sorting into exosomes and extracellular vesicles. Biochim Biophys Acta Proteins Proteom. 2019;1867(12):140203.

24. Zaborowski MP, Balaj L, Breakefield XO, Lai CP. Extracellular vesicles: composition, Biological relevance, and methods of study. Bioscience. 2015;65(8):783–97.

25. Samuvel DJ, Li L, Krishnasamy Y, Gooz M, Takemoto K, Woster PM, Lemasters JJ, Zhong Z. Mitochondrial depolarization after acute ethanol treatment drives mitophagy in living mice. Autophagy. 2022;18(11):2671–85.

26. Boyapati RK, Tamborska A, Dorward DA, Ho GT. Advances in the understanding of mitochondrial DNA as a pathogenic factor in inflammatory diseases. F1000Res. 2017;6:169.

27. Qian F, Huang Z, Zhong H, Lei Q, Ai Y, Xie Z, Zhang T, Jiang B, Zhu W, Sheng Y, et al. Analysis and Biomedical Applications of Functional Cargo in Extracellular vesicles. ACS Nano. 2022;16(12):19980–20001.

28. O'Brien K, Ughetto S, Mahjoum S, Nair AV, Breakefield XO. Uptake, functionality, and re-release of extracellular vesicle-encapsulated cargo. Cell Rep. 2022;39(2):110651.

29. Vu K, Weksler B, Romero I, Couraud PO, Gelli A. Immortalized human brain endothelial cell line HCMEC/D3 as a model of the blood-brain barrier facilitates in vitro studies of central nervous system infection by Cryptococcus neoformans. Eukaryot Cell. 2009;8(11):1803–7.

30. Soo CY, Song Y, Zheng Y, Campbell EC, Riches AC, Gunn-Moore F, Powis SJ. Nanoparticle tracking analysis monitors microvesicle and exosome secretion from immune cells. Immunology. 2012;136(2):192–7.

31. Lazo S, Noren Hooten N, Green J, Eitan E, Mode NA, Liu QR, Zonderman AB, Ezike N, Mattson MP, Ghosh P, et al. Mitochondrial DNA in extracellular vesicles declines with age. Aging Cell. 2021;20(1):e13283.

32. Sluyter R. The P2X7 Receptor. Adv Exp Med Biol. 2017;1051:17–53.

33. Zhai K, Liskova A, Kubatka P, Busselberg D. Calcium entry through TRPV1: a potential target for the regulation of proliferation and apoptosis in cancerous and healthy cells. Int J Mol Sci. 2020;21(11):4117.

34. Groenendyk J, Agellon LB, Michalak M. Calcium signaling and endoplasmic reticulum stress. Int Rev Cell Mol Biol. 2021;363:1–20.

35. Thomas KC, Sabnis AS, Johansen ME, Lanza DL, Moos PJ, Yost GS, Reilly CA. Transient receptor potential vanilloid 1 agonists cause endoplasmic reticulum stress and cell death in human lung cells. J Pharmacol Exp Ther. 2007;321(3):830–8.

36. Gorlach A, Klappa P, Kietzmann T. The endoplasmic reticulum: folding, calcium homeostasis, signaling, and redox control. Antioxid Redox Signal. 2006;8(9–10):1391–418.

37. Zeeshan HM, Lee GH, Kim HR, Chae HJ. Endoplasmic reticulum stress and Associated ROS. Int J Mol Sci. 2016;17(3):327.

38. Norgard MO, Lund PM, Kalisi N, Andresen TL, Larsen JB, Vogel S, Svenningsen P. Mitochondrial reactive oxygen species modify extracellular vesicles secretion rate. FASEB BioAdvances. 2023;5(9):355–66.

39. Vujic T, Schvartz D, Furlani IL, Meister I, Gonzalez-Ruiz V, Rudaz S, Sanchez JC. Oxidative stress and Extracellular Matrix Remodeling are signature pathways of Extracellular vesicles released upon Morphine exposure on human brain microvascular endothelial cells. Cells. 2022;11(23):3926.

40. Andres J, Smith LC, Murray A, Jin Y, Businaro R, Laskin JD, Laskin DL. Role of extracellular vesicles in cell-cell communication and inflammation following exposure to pulmonary toxicants. Cytokine Growth Factor Rev. 2020;51:12–8.

41. Rahman MA, Patters BJ, Kodidela S, Kumar S. Extracellular vesicles: intercellular mediators in Alcohol-Induced pathologies. J Neuroimmune Pharmacol. 2020;15(3):409–21.

42. Rossol M, Pierer M, Raulien N, Quandt D, Meusch U, Rothe K, Schubert K, Schoneberg T, Schaefer M, Krugel U, et al. Extracellular Ca2 + is a danger signal activating the NLRP3 inflammasome through G protein-coupled calcium sensing receptors. Nat Commun. 2012;3:1329.

43. Conte G, Menendez-Mendez A, Bauer S, El-Naggar H, Alves M, Nicke A, Delanty N, Rosenow F, Henshall DC, Engel T. Circulating P2X7 Receptor Signaling Components as Diagnostic Biomarkers for Temporal Lobe Epilepsy. Cells. 2021;10(9):2444.

44. Thornton C, Grad E, Yaka R. The role of mitochondria in cocaine addiction. Biochem J. 2021;478(4):749–64.

45. Song BJ, Akbar M, Abdelmegeed MA, Byun K, Lee B, Yoon SK, Hardwick JP. Mitochondrial dysfunction and tissue injury by alcohol, high fat, nonalcoholic substances and pathological conditions through post-translational protein modifications. Redox Biol. 2014;3:109–23.

46. Deng H, Zhang Y, Li GG, Yu HH, Bai S, Guo GY, Guo WL, Ma Y, Wang JH, Liu N, et al. P2X7 receptor activation aggravates NADPH oxidase 2-induced oxidative stress after intracerebral hemorrhage. Neural Regen Res. 2021;16(8):1582–91.

47. Panday A, Sahoo MK, Osorio D, Batra S. NADPH oxidases: an overview from structure to innate immunity-associated pathologies. Cell Mol Immunol. 2015;12(1):5–23.

48. Veith A, Moorthy B. Role of cytochrome P450s in the generation and metabolism of reactive oxygen species. Curr Opin Toxicol. 2018;7:44–51.

49. Park J, Lee J, Choi C. Mitochondrial network determines intracellular ROS dynamics and sensitivity to oxidative stress through switching inter-mitochondrial messengers. PLoS ONE. 2011;6(8):e23211.

50. Baudelet D, Lipka E, Millet R, Ghinet A. Involvement of the P2X7 purinergic receptor in inflammation: an update of antagonists series since 2009 and their promising therapeutic potential. Curr Med Chem. 2015;22(6):713–29.

51. Wang J, Yu Y. Insights into the channel gating of P2X receptors from structures, dynamics and small molecules. Acta Pharmacol Sin. 2016;37(1):44–55.

52. Sluyter R, Stokes L. Significance of P2X7 receptor variants to human health and disease. Recent Pat DNA Gene Seq. 2011;5(1):41–54.

53. Di Virgilio F, Dal Ben D, Sarti AC, Giuliani AL, Falzoni S. The P2X7 Receptor in Infection and Inflammation. Immunity. 2017;47(1):15–31.

54. Wilkaniec A, Cieslik M, Murawska E, Babiec L, Gassowska-Dobrowolska M, Palasz E, Jesko H, Adamczyk A. P2X7 receptor is involved in mitochondrial Dysfunction Induced by Extracellular Alpha Synuclein in Neuroblastoma SH-SY5Y cells. Int J Mol Sci. 2020;21(11):3959.

55. Potula R, Gentile TA, Meissler JJ, Shekarabi A, Wiah S, Farkas DJ, Inan S, Eisenstein TK, Rawls SM. Purinergic P2X7 receptor antagonist inhibits methamphetamine-induced reward, hyperlocomotion, and cortical IL-7A levels in mice: A role for P2X7/IL-17A crosstalk in methamphetamine behaviors? Brain Behav Immun. 2023;107:47–52.

56. Schneider S, Merfort I, Idzko M, Zech A. Blocking P2X purinoceptor 4 signalling alleviates cigarette smoke induced pulmonary inflammation. Respir Res. 2022;23(1):148.

57. Wang M, Zhang Y, Xu M, Zhang H, Chen Y, Chung KF, Adcock IM, Li F. Roles of TRPA1 and TRPV1 in cigarette smoke -induced airway epithelial cell injury model. Free Radic Biol Med. 2019;134:229–38.

58. Vardanyan A, Wang R, Vanderah TW, Ossipov MH, Lai J, Porreca F, King T. TRPV1 receptor in expression of opioid-induced hyperalgesia. J Pain. 2009;10(3):243–52.

59. Papa R, Penco F, Volpi S, Gattorno M. Actin remodeling defects leading to Autoinflammation and Immune Dysregulation. Front Immunol. 2020;11:604206.

60. Daverkausen-Fischer L, Prols F. Regulation of calcium homeostasis and flux between the endoplasmic reticulum and the cytosol. J Biol Chem. 2022;298(7):102061.

61. Bagur R, Hajnoczky G. Intracellular ca(2+) sensing: its role in Calcium Homeostasis and Signaling. Mol Cell. 2017;66(6):780–8.

62. Zhai X, Sterea AM, Hiani YE. Lessons from the endoplasmic reticulum ca(2+) Transporters-A Cancer connection. Cells. 2020;9(6):1536.

63. Park SW, Zhou Y, Lee J, Lee J, Ozcan U. Sarco(endo)plasmic reticulum Ca2+-ATPase 2b is a major regulator of endoplasmic reticulum stress and glucose homeostasis in obesity. Proc Natl Acad Sci U S A. 2010;107(45):19320–5.

64. Riaz TA, Junjappa RP, Handigund M, Ferdous J, Kim HR, Chae HJ. Role of endoplasmic reticulum stress Sensor IRE1alpha in Cellular Physiology, Calcium, ROS Signaling, and metaflammation. Cells. 2020;9(5):1160.

65. Preissler S, Rato C, Yan Y, Perera LA, Czako A, Ron D. Calcium depletion challenges endoplasmic reticulum proteostasis by destabilising BiP-substrate complexes. Elife. 2020;9:e62601.

66. Acosta-Alvear D, Karagoz GE, Frohlich F, Li H, Walther TC, Walter P. The unfolded protein response and endoplasmic reticulum protein targeting machineries converge on the stress sensor IRE1. Elife. 2018;7:e43036.

67. Mathuranyanon R, Tsukamoto T, Takeuchi A, Ishiwata-Kimata Y, Tsuchiya Y, Kohno K, Kimata Y. Tight regulation of the unfolded protein sensor Ire1 by its intramolecularly antagonizing subdomain. J Cell Sci. 2015;128(9):1762–72.

68. Kadowaki H, Nishitoh H. Signaling pathways from the endoplasmic reticulum and their roles in disease. Genes. 2013;4(3):306–33.

69. Lee GH, Lee HY, Li B, Kim HR, Chae HJ. Bax inhibitor-1-mediated inhibition of mitochondrial Ca2 + intake regulates mitochondrial permeability transition pore opening and cell death. Sci Rep. 2014;4:5194.

70. Zhang D, Armstrong JS. Bax and the mitochondrial permeability transition cooperate in the release of cytochrome c during endoplasmic reticulum-stress-induced apoptosis. Cell Death Differ. 2007;14(4):703–15.

71. Wong CH, Chen YC. Clinical significance of exosomes as potential biomarkers in cancer. World J Clin Cases. 2019;7(2):171–90.

72. Wu F, Yin Z, Yang L, Fan J, Xu J, Jin Y, Yu J, Zhang D, Yang G. Smoking Induced Extracellular vesicles Release and their distinct properties in Non-small Cell Lung Cancer. J Cancer. 2019;10(15):3435–43.

73. Mobarrez F, Antoniewicz L, Hedman L, Bosson JA, Lundback M. Electronic cigarettes containing nicotine increase endothelial and platelet derived extracellular vesicles in healthy volunteers. Atherosclerosis. 2020;301:93–100.

74. Zhu J, Liu B, Wang Z, Wang D, Ni H, Zhang L, Wang Y. Exosomes from nicotine-stimulated macrophages accelerate atherosclerosis through miR-21-3p/PTEN-mediated VSMC migration and proliferation. Theranostics. 2019;9(23):6901–19.

75. Ibanez F, Montesinos J, Urena-Peralta JR, Guerri C, Pascual M. TLR4 participates in the transmission of ethanol-induced neuroinflammation via astrocyte-derived extracellular vesicles. J Neuroinflammation. 2019;16(1):136.

76. Chandra R, Engeln M, Schiefer C, Patton MH, Martin JA, Werner CT, Riggs LM, Francis TC, McGlincy M, Evans B, et al. Drp1 mitochondrial fission in D1 neurons mediates behavioral and Cellular plasticity during early Cocaine abstinence. Neuron. 2017;96(6):1327–1341e1326.

77. Wen S, Aki T, Funakoshi T, Unuma K, Uemura K. Role of Mitochondrial Dynamics in Cocaine's Neurotoxicity. Int J Mol Sci 2022; 23(10).

78. Pfeiffer ZA, Aga M, Prabhu U, Watters JJ, Hall DJ, Bertics PJ. The nucleotide receptor P2X7 mediates actin reorganization and membrane blebbing in RAW 264.7 macrophages via p38 MAP kinase and Rho. J Leukoc Biol. 2004;75(6):1173–82.

79. Le Dare B, Ferron PJ, Gicquel T. The Purinergic P2X7 Receptor-NLRP3 Inflammasome Pathway: A New Target in Alcoholic Liver Disease? Int J Mol Sci. 2021;22(4):2139.

80. Corriden R, Insel PA. Basal release of ATP: an autocrine-paracrine mechanism for cell regulation. Sci Signal. 2010;3(104):re1.

81. Drago F, Lombardi M, Prada I, Gabrielli M, Joshi P, Cojoc D, Franck J, Fournier I, Vizioli J, Verderio C. ATP modifies the Proteome of Extracellular vesicles released by Microglia and influences their action on astrocytes. Front Pharmacol. 2017;8:910.

82. Svitkina T. The actin cytoskeleton and actin-based motility. Cold Spring Harb Perspect Biol. 2018;10(1):a018267.

83. D'Acunzo P, Ungania JM, Kim Y, Barreto BR, DeRosa S, Pawlik M, Canals-Baker S, Erdjument-Bromage H, Hashim A, Goulbourne CN, et al. Cocaine perturbs mitovesicle biology in the brain. J Extracell Vesicles. 2023;12(1):e12301.

84. Di Mambro T, Pellielo G, Agyapong ED, Carinci M, Chianese D, Giorgi C, Morciano G, Patergnani S, Pinton P, Rimessi A. The tricky connection between Extracellular vesicles and Mitochondria in Inflammatory-Related diseases. Int J Mol Sci. 2023;24(9):8181.

85. Tkach M, Thery C. Communication by Extracellular vesicles: where we are and where we need to go. Cell. 2016;164(6):1226–32.

86. Colombo M, Raposo G, Thery C. Biogenesis, secretion, and intercellular interactions of exosomes and other extracellular vesicles. Annu Rev Cell Dev Biol. 2014;30:255–89.

87. MacKenzie A, Wilson HL, Kiss-Toth E, Dower SK, North RA, Surprenant A. Rapid secretion of interleukin-1beta by microvesicle shedding. Immunity. 2001;15(5):825–35.

88. Pizzirani C, Ferrari D, Chiozzi P, Adinolfi E, Sandona D, Savaglio E, Di Virgilio F. Stimulation of P2 receptors causes release of IL-1beta-loaded microvesicles from human dendritic cells. Blood. 2007;109(9):3856–64.

89. Wu H, Nie Y, Xiong H, Liu S, Li G, Huang A, Guo L, Wang S, Xue Y, Wu B, et al. P2X7 Receptor Expression in Peripheral Blood Monocytes Is Correlated With Plasma C-Reactive Protein and Cytokine Levels in Patients With Type 2 Diabetes Mellitus: a Preliminary Report. Inflammation. 2015;38(6):2076–81.

90. Garcia-Villalba J, Hurtado-Navarro L, Penin-Franch A, Molina-Lopez C, Martinez-Alarcon L, Angosto-Bazarra D, Baroja-Mazo A, Pelegrin P. Soluble P2X7 Receptor Is Elevated in the Plasma of COVID-19 Patients and Correlates With Disease Severity. Front Immunol. 2022;13:894470.

91. Pelegrin P. P2X7 receptor and the NLRP3 inflammasome: Partners in crime. Biochem Pharmacol. 2021;187:114385.

92. Savage CD, Lopez-Castejon G, Denes A, Brough D. NLRP3-Inflammasome activating DAMPs stimulate an inflammatory response in Glia in the absence of Priming which contributes to brain inflammation after Injury. Front Immunol. 2012;3:288.

93. Horng T. Calcium signaling and mitochondrial destabilization in the triggering of the NLRP3 inflammasome. Trends Immunol. 2014;35(6):253–61.

94. Lee GS, Subramanian N, Kim AI, Aksentijevich I, Goldbach-Mansky R, Sacks DB, Germain RN, Kastner DL, Chae JJ. The calcium-sensing receptor regulates the NLRP3 inflammasome through Ca2 + and cAMP. Nature. 2012;492(7427):123–7.

95. Gellatly S, Pavelka N, Crue T, Schweitzer KS, Day BJ, Min E, Numata M, Voelker DR, Scruggs A, Petrache I, et al. Nicotine-free e-Cigarette vapor exposure stimulates IL6 and mucin production in human primary small Airway Epithelial cells. J Inflamm Res. 2020;13:175–85.

96. Caporale A, Langham MC, Guo W, Johncola A, Chatterjee S, Wehrli FW. Acute effects of electronic cigarette aerosol inhalation on vascular function detected at quantitative MRI. Radiology. 2019;293(1):97–106.

97. Boulay ME, Henry C, Bosse Y, Boulet LP, Morissette MC. Acute effects of nicotine-free and flavour-free electronic cigarette use on lung functions in healthy and asthmatic individuals. Respir Res. 2017;18(1):33.

Publisher's Note

Springer Nature remains neutral with regard to jurisdictional claims in published maps and institutional affiliations.